Preparation of Mesoporous SiO_2 and ZnO•SiO_2 Composite from Raw Rice Husk for Removal of Organic Dye

Le Tien Dat, Hoang Thi Thu, Nguyen Thi Van, Vu Anh Tuan*

Hanoi University of Science and Technology – No. 1, Dai Co Viet Str., Hai Ba Trung, Ha Noi, Viet Nam

Received: October 26, 2018; Accepted: June 24, 2019

Abstract

Mesoporous SiO_2 and ZnO•SiO_2 composite (10 wt.% of SiO_2) were prepared from rice husk for removal of organic dye (Janus Green B, JGB). As-prepared samples were characterized by XRD, FE-SEM, FT-IR, and N_2 adsorption/desorption isotherms. SiO_2 was observed as mesoporous material with large surface area (98.2 m^2/g) and high pore volume (0.746 cm^3/g). However, these values were significantly decreased when ZnO doped in ZnO•SiO_2 composite. The performance of SiO_2 was evaluated by adsorption of JGB and performance of ZnO•SiO_2 composite was evaluated by photo-degradation of JGB under low UV intensity (8 W). The adsorption capacity of SiO_2 was 3379.5 mg/g and adsorption rate was 0.062 min^{-1}. The degradation efficiency of JGB on ZnO•SiO_2 composite was 97.9% in 60 min and degradation rate was 0.061 min^{-1}.

Keywords: Photo-degradation, Zinc oxide, Mesoporous silica, Rice Husk, Janus green B

1. Introduction

Industrial wastewater can contain a wide range of pollutants such as organic compounds and heavy metals. It can have a significant impact on human health and environmental disasters if it is untreated and discharged directly into the environment. Industries must be responsible for ensuring the quality of the effluent within acceptable standards. However, The UN World Water Development Report, in many developing countries, more than 70 percent of unprocessed industrial waste is discharged into water sources and contaminated water [1]. The largest sources of hazardous industrial wastewater come from mining, pulp mill, textiles, tanning, sugar mills and pharmaceutical manufacturing [2]. In many cases, industrial wastewater not only discharges directly but also infiltrates the ground causing groundwater contamination and underground wells. Therefore, industrial effluents need to be treated before being delivered to the environment.

The semiconductor photocatalysis has emerged as one of the most promising processes for wastewater treatment as compared to other conventional techniques [3]. In which, ZnO with high stability, photosensitivity, advanced optical properties, and low cost is an excellent selection for wastewater treatment process [4,5]. When, ZnO nano particles were deposited on porous materials such as SiO_2, AC (activated carbon), and MOF (metal organic framework), the catalytic activity and adsorption capacity could be increased [6-8].

Recently, metal containing mesoporous silica have attracted much attention because the silica-based materials have the high surface area, good thermal stability, and favorable hydrothermal stability. Numerous iron mesoporous silica composites were synthesized for degrading organic compounds such as methyl orange, acid orange, polyarylamide, and phenol [9-12]. The selection of suitable silica source is a crucial factor with respect to practical application because the silica source is directly affected not only to properties of silica supporters but to cost effective application. Mesoporous silica synthesized by using tetraethyl orthosilicate (TEOS) was known as a relatively expense silica material. In this study, rice husk (RH), a cheap silica source, was utilized, which is a by-product from rice mills in enormous quantities. As an energy source in various industries burning rice husk generates rice husk ash (RHA) that contains a high percentage of silica and can be an economically valuable raw material for production of natural silica.

In this study, mesoporous SiO_2 was prepared from RH and ZnO•SiO_2 composite was prepared by hydrothermal method. As-prepared samples were characterized by FE-SEM, XRD, BET and FT-IR. The performance SiO_2 was evaluated by the adsorption of JGB and the performance of ZnO•SiO_2 composite was

* Corresponding author: Tel.: (+84) 912.911.902
Email: tuan.vuanh@hust.edu.vn

evaluated by photo-degradation of JGB.

2. Experimental

2.1. Materials

Janus Green B (JGB) was purchased from Sigma-Aldrich, the chemical structure and basic physicochemical properties of JGB are presented in Fig.1. Rice husk was obtained from Hung Cuc Co., LTD, Đông Hưng, Thai Binh, Vietnam. Zinc acetate (99.0), hexamethylene tetramine-HMTA ($C_6H_{12}N_4$), sodium hydroxide (99.5 %), liquid ammonia (28%), cetyl trimetylammonium bromua (CTAB) were obtained from Merck. Double distilled water was used at all the experiments. The pH of the solution was adjusted by using dilute solutions of H_2SO_4 and NaOH.

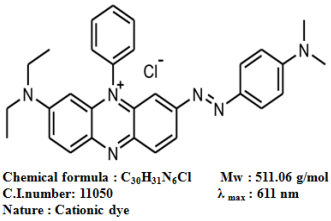

Fig. 1. The chemical structure and physical properties of JGB.

2.2. Preparation of silica from rice husk

The preparation of silica is presented in Fig.2(a). RH obtained from Hung Cuc Co., LTD, Đông Hưng, Thai Binh was washed with tap water, then it was further rinsed with distilled water up to 5 times. The washed rice husk was separately treated with HCl 0.5 M for 30 minutes with constant stirring. After the acidic solution was drained off, the rice husk was rinsed with distilled water until free from acids, filtered and dried in air at 80 °C for 24 h. Then, it was burned in a muffle furnace at 600 °C for 2 h to obtain RHA. After that, 5 g of RHA was mixed with 100 mL NaOH 2M in an Erlenmeyer flask, the mixture was boiled for 2h to dissolve silica from ash. The Na_2SiO_3 was formed by following reaction:

$$SiO_{2\ RHA} + 2NaOH \rightarrow Na_2SiO_3 + H_2O \qquad (1)$$

The slurry consisting of residue digested ash, Na_2SiO_3, water and free NaOH was then filtered and the colorless filtrated solution with pH of about 13 was cool to room temperature.

The mixture of 0.219 g of CTAB and 34 mL of HCl 0.6 N were stirred for 5 min. 40 mL of Na_2SiO_3 prepared at the previous step was added into mixture, the pH solution was adjusted at 7.5÷8.5 by HCl and NaOH solutions and stirred for 1 h. The mixture was aged at 50 °C for 24 h to form white gel, and then it was poured in an autoclave at 100 °C for 48 h. The white solid was recovered by filtration and washing with distilled water to remove the excess amount of surfactant until measuring neutral pH. Finally, mesoporous silica was obtained after drying at 100 °C overnight and calcined at 600 °C for 6 h.

2.3. Preparation of ZnO•SiO₂

The $ZnO•SiO_2$ composite was prepared by hydrothermal method and the preparation procedure is presented in Fig.2 (b). Typically, 2.19 g zinc acetate and 0.7 g HMTA were dissolved in 100 mL of distilled water to form clear solution. Subsequently, the pH of solution was adjusted to 8.0 by using liquid ammonia.

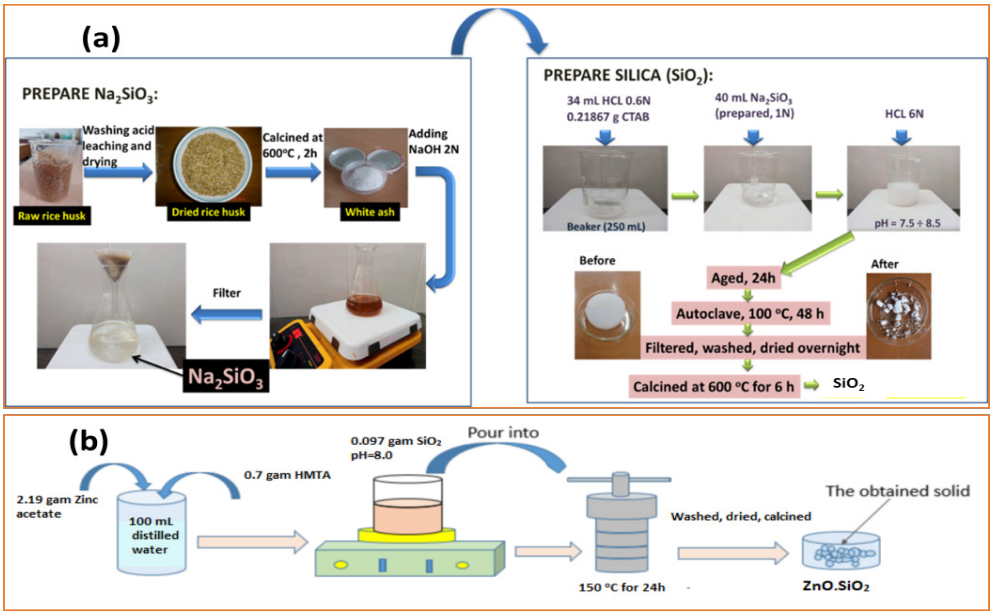

Fig. 2. (a) Preparation procedure of mesoporous silica and (b) preparation procedure of $ZnO•SiO_2$

After 5 minutes of stirring, the 0.097 g of SiO_2, corresponding to 10 wt.% of SiO_2, was added to above solution. The suspension was stirred vigorously for 5 min and then transferred into autoclave and heated at 150 °C for 24 h. The resulting solids were washed several times with distilled water and dried at 80 °C for 24 h. Finally, the white powder was calcined in air at 600 °C for 6 h to obtained ZnO•SiO_2 composite. For comparison, the ZnO was prepared by the same procedure with ZnO•SiO_2 without addition of SiO_2.

2.4. Characterization

The crystalline phase of samples was investigated by X-ray power diffraction. XRD patterns were obtained by using Bruker D8 Ax XRD-diffractometer (Germany) with Cu Kα irradiation (40kV, 40 mA). The 2θ ranging from 10 to 80 ° was selected to analyse the crystal structure. The morphology of the samples was observed by field emission scanning electron microscopy (FE-SEM, JEOL-7600F). The textural properties were measured via N_2 adsorption/desorption isotherms using a Micromeritics (Gemini VII analyzer). The specific surface area was obtained by using the Brunauer-Emmett-Teller (BET) method. The Fourier transform infrared spectroscopy (FTIR) was measured by Madison equiment (WI, USA).

3. Results and discussion

3.1. Characterization of samples

3.1.1. FE-SEM analysis

The surface morphologies of the as-prepared samples were studied using Field Emission Scanning Electron Microscope and the results are presented in Fig.3. Silica showed an irregular polyhedral shape, like light clouds in Fig.3(a), the SiO_2 particles with the ragged surface were around 20-40 nm in size in Fig.3(b). The unique microporous structure and environmental friendly characteristics make SiO_2 as an excellent candidate for supporter or adsorbent. By the hydrothermal method, it could be observed that ZnO with rod-like shape was relatively dispersed on composite. The bulk shape of ZnO had average length of about 2-3 μm and width of about 200-300 nm in Fig.3(c) and (d)

3.1.2. XRD analysis

Fig.4 shows the XRD patterns of SiO_2 and ZnO•SiO_2 composite. The XRD pattern of SiO_2 showed two broad peaks at 2θ of 14 and 23°, indicating that as-prepared SiO_2 was amorphous material. And, there was no other peaks observed, implying the purity of SiO_2. For composite, the diffraction peaks at 2θ=31.8; 34.5; 36.3, 47.6, 56.6, 62.8, 67.9, and 69.1° corresponding to 100, 202, 101, 102, 110, 103, 112 and 201 plans could be attributed to crystallite of hexagonal wurtzite phase ZnO (JCPDS No. 00-036-1451). The narrow sharp peaks indicated that the ZnO was high crystallinity, implying the high purity of as-prepared ZnO•SiO_2 composite [13-15].

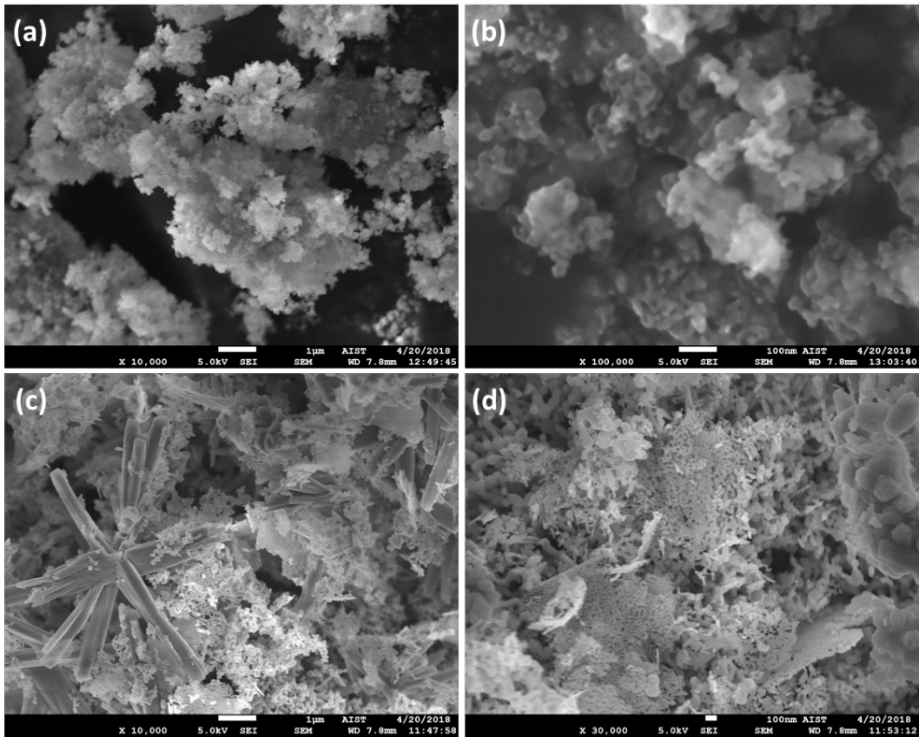

Fig. 3. (a-b) FE-SEM images of SiO_2 and (c-d) FE-SEM images of ZnO•SiO_2 composite.

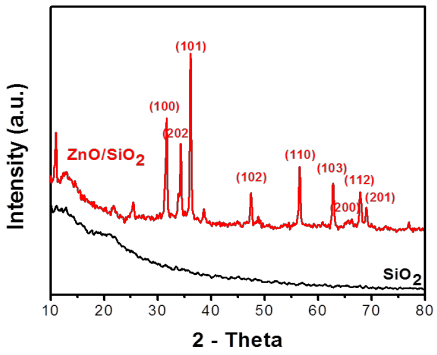

Fig. 4. XRD patterns of SiO_2 and ZnO•SiO_2 composite

3.1.3. N_2 adsorption/desorption isotherms

The N_2 adsorption/desorption isotherms and the pore size distributions of SiO_2 and ZnO•SiO_2 are shown in Fig.5. The N_2 adsorption/desorption isotherm of SiO_2 was a type IV with a type H1 hysteresis loop according to the IUPAC classification, indicating mesopore a well-defined cylindrical-like pore channels. The hysteresis of the SiO_2 sample was observed at relative pressure (p/p_o) of 0.82 to 1.0. The surface area, pore volume, and average pore size of SiO_2 were 98.2m^2/g, 0.746 cm^3/g and 28.8 nm, respectively, as presented in Table 1. These data showed that SiO_2 had large surface area and pore volume, confirming their stronger adsorption ability and great potential for application as a carrier.

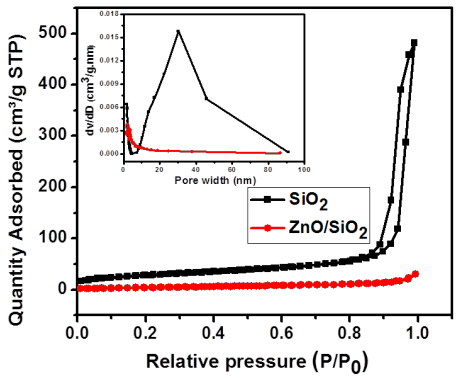

Fig. 5. N_2 adsorption/desorption isotherms (inset: pore size distributions) of SiO_2 and ZnO•SiO_2 composite.

For composite, after ZnO loading by hydrothermal method, the hysteresis became smaller, the pore size distribution became broader. These results led the significant decrease in surface area and pore volume of composite, 16.6 m^2/g and 0.047 cm^3/g, respectively. In addition, the average pore size was smaller than that of SiO_2. The significant reduction of surface area and pore volume was assigned to the size of ZnO particles was relative larger than SiO_2 particles. These confirmed that ZnO particles was successfully loaded on amorphous SiO_2.

Table 1. Textural properties of SiO_2 and ZnO•SiO_2 composite.

Samples	S_{BET} (m^2/g)	BJH Pore volume (cm^3/g)	Average pore size (nm)
SiO_2	98.2	0.746	28.8
ZnO•SiO_2	16.6	0.047	10.0

3.1.4. FT-IR analysis

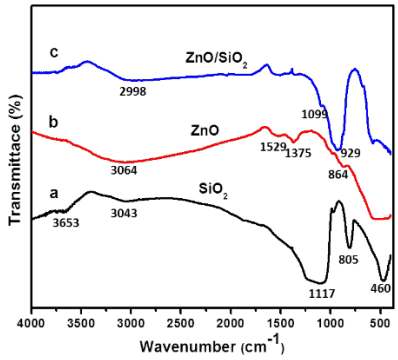

Fig. 6. FT-IR spectra of SiO_2, ZnO and ZnO•SiO_2 composite powder.

The FT-IR was used to analyze the chemical groups of a sample and also to assess whether a chemical reaction took place between ZnO and amorphous SiO_2. The FT-IR spectra of as-synthesized SiO_2 can be seen in Fig.6(a). The bands near 3653 and 3043 cm^{-1} corresponded to the O-H stretching vibration of Si-O-H and absorbed water (H-O-H) [16]. The intense bands at 1117, 805 and 460 cm^{-1} could be assigned to the Si-O-Si asymmetric stretching vibrations [17]. As seen in Fig.6(b), the stretching mode of the Zn-O bond can be seen in the range spanning from 540 to 570 cm^{-1}, the peak at 1529 cm^{-1} could be attributed to vibration of C=O [18]. As seen in Fig.6(c), the vibration bands found at 1099 and 929 cm^{-1} could be assigned to the stretching vibration of Zn-O and Si-O-Zn, respectively, which confirmed that SiO_2 indeed binds with ZnO.

3.2. Adsorption of JGB on SiO_2

The relation of adsorption efficiency for pollutants from aqueous solution of adsorbent versus time is important to the design and optimization of an adsorption system. In this study, the effect of contact time on adsorption efficiency was investigated by a batch test. Typically, 0.025 g of SiO_2 was added into 100 mL of JGB 10 mg/L, pH solution was adjusted at

7.0 by NaOH and H_2SO_4, the experiment was carried out at room temperature. At given time intervals, 2 mL of samples were withdrawn from the suspension and then filtered by a syringe filter (0.45 µm PTFE membrane) to remove the catalyst. The dye concentration of the filtrate was analyzed by a UV-Vis spectrophotometer (Agilent 8453) at the maximum absorbance wavelength 611 nm. The equilibrium sorption capacity (q_e) and the removal efficiency (Re) were determined by following equations [19]:

$$q_e = \frac{(C_o - C_e)\times V}{m} \qquad (2)$$

$$Re = \frac{C_0 - C_t}{C_0} \times 100\% \qquad (3)$$

Where C_o (mg/L) is the initial dye concentration, C_e (mg/L) is the dye concentration at equilibrium and C_t (mg/L) is the concentration at adsorption time t, V is the volume of dye solution (L), m is the mass of the adsorbent (g).

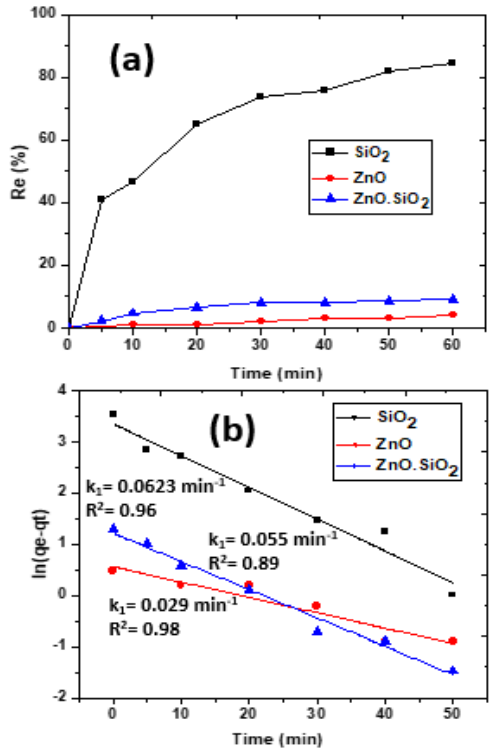

Fig. 7. (a) adsorption of JGB on mesoporous SiO_2, ZnO and ZnO•SiO_2 and (b) fitting plots of pseudo-first-order kinetic model.

Fig.7(a) shows the plots of adsorption of JGB on mesoporous SiO_2, ZnO and ZnO•SiO_2. The adsorption abilities of ZnO and ZnO•SiO_2 with JBG were small, the removal efficiencies were 5.10 and 9.11 %, receptivity. The removal efficiency of JGB on SiO_2 gradually increased with time and the adsorption achieved saturation at 60 min, with the removal efficiency of 84.48% and the adsorption capacity of SiO_2 was 3379.5 mg/g.

The study of chemical kinetics can provide important information on adsorption rate and the factors affecting the sorption rate. In order to investigate the mechanism of dye adsorption on SiO_2, the pseudo-first-order model was used.

$$ln(q_e - q_t) = lnq_e - k_1.t \qquad (4)$$

Where q_e and q_t are the adsorption amount of JGB (mg/g) at time t and equilibrium, respectively, k_1(min^{-1}) is the rate constant. The values of k_1 and q_e can be determined from the plot of $ln(q_e - q_t)$ versus t.

Fig.7(b) presents the plot of pseudo-first-order kinetic model. It showed the good fitting with the coefficient values (R^2) were larger than 0.89. The rate constants (k_1) were 0.062, 0.029, and 0.055 min^{-1} for SiO_2, ZnO and ZnO•SiO_2, respectively.

3.3. Photo-degradation of JGB on the ZnO•SiO_2 composite

The photo-degradation of JGB on catalyst was also carried out by batch test. Typically, 50 mg of catalyst was added into a 250 mL glass beaker containing 100 mL of JGB 10 mg/L. The mixed solution was ultrasonicated for 10 min and then the UV lamp (8W halogen lamp) was switched on. The catalyst powders were stirred at a constant rate entire reaction process. At given time intervals of 10 min, the solution was filtered and the concentration was measured by the same procedure with section 3.2. The degradation efficiency was calculated by following equation:

$$De\ (\%) = \frac{C_0 - C_t}{C_0}.100\% \qquad (5)$$

The photo-degradation rate of JGB on catalysts can be evaluated by using the pseudo-first-order model as follow:

$$ln\frac{C_0}{C_t} = k.t \qquad (6)$$

Where C_o and C_t are the concentrations of JGB at initial (t =0) and time t (min), respectively. k is the pseudo first-order rate constant. The k value was calculated from the slope of the ln (C_o/C_t) versus t plot.

Fig.8(a) shows the degradation of JGB on the SiO_2, ZnO and ZnO•SiO_2 composite within 60 min. The degradation of JGB on SiO_2 could be neglected. The degradation of JGB on ZnO•SiO_2 was lager than that of ZnO, the degradation efficiencies in 60 min were 97.9 and 84.9% for ZnO•SiO_2 and ZnO, respectively. Fig.8(b) shows the kinetic curves for degradation of JGB. The experiment profile was good fitting with pseudo-first-order model. The reaction rates (k_1) were $6.7.10^{-4}$, 0.037, and 0.061 min^{-1} for SiO_2, ZnO and ZnO•SiO_2, respectively.

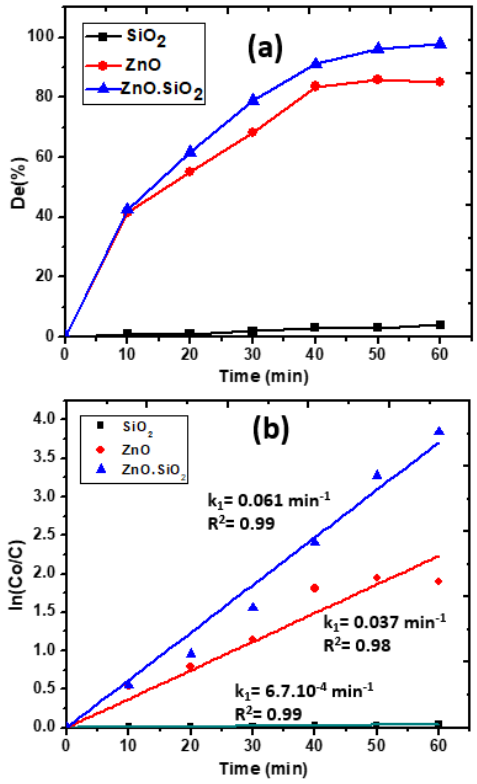

Fig. 8. (a) Photo-degradation of JGB on mesoporous SiO_2, ZnO and ZnO•SiO_2 and (b) fitting plots of pseudo-first-order kinetic model.

4. Conclusion

In summary, mesoporous SiO_2 and ZnO•SiO_2 composite (10 wt.% of SiO_2) were successfully prepared from rice husk. With the assistant of the surfactant CTAB, SiO_2 was observed as mesoporous material with large surface area (98.2 m^2/g) and high pore volume (0.746 cm^3/g). The hysteresis became smaller and the pore size distribution became broader after ZnO loading on ZnO•SiO_2 composite. As the results, the surface area and pore volume were significantly decreased. The SiO_2 sample showed the high adsorption ability as compared to ZnO and ZnO•SiO_2. The adsorption capacity of SiO_2 was 3379.5 mg/g and adsorption rate was 0.062 min^{-1}. Whereas, the degradation efficiency of JGB on ZnO•SiO_2 composite in 60 min (97.9%) was higher than those of SiO_2 and ZnO.

Acknowledgements

We are gratefully acknowledged for financial support of Vietnamese Ministry of Education and Training by the Grant number of B2017-BKA-53.

References

[1] T.U.W.W.D. Report, Water for a Sustainable World, 2015.

[2] G. Moussavi, M. Mahmoudi; Removal of azo and anthraquinone reactive dyes from industrial wastewaters using MgO nanoparticles; Journal of Hazardous Materials 168 (2009) 806-812.

[3] Q. Zhu, W.-S. Wang, L. Lin, G.-Q. Gao, H.-L. Guo, H. Du, A.-W. Xu; Facile Synthesis of the Novel Ag3VO4/AgBr/Ag Plasmonic Photocatalyst with Enhanced Photocatalytic Activity and Stability; The Journal of Physical Chemistry C 117 (2013) 5894-5900.

[4] Z.-g. Jia, K.-k. Peng, Y.-h. Li, R.-s. Zhu; Preparation and photocatalytic performance of porous ZnO microrods loaded with Ag; Transactions of Nonferrous Metals Society of China 22 (2012) 873-878.

[5] T. Thangeeswari, A.T. George, A. Arun Kumar; Optical Properties and FTIR Studies of Cobalt Doped ZnO Nanoparticles by Simple Solution Method, 2016.

[6] A.M. Ali, A.A. Ismail, R. Najmy, A. Al-Hajry;, Preparation and characterization of ZnO–SiO_2 thin films as highly efficient photocatalyst, Journal of Photochemistry and Photobiology A: Chemistry 275 (2014) 37-46.

[7] S.J. Yang, J.H. Im, T. Kim, K. Lee, C.R. Park; MOF-derived ZnO and ZnO@C composites with high photocatalytic activity and adsorption capacity, Journal of Hazardous Materials 186 (2011) 376-382.

[8] N.T. Van, V.a. Tuan; Photo-degradation of Janus Green B on zince oxide nano particles loaded on activated carbon preparation from rice husk; Vietnam Journal of Chemistry Vol. 56 (2018) 306-311.

[9] N. Panda, H. Sahoo, S. Mohapatra; Decolourization of Methyl Orange using Fenton-like mesoporous Fe_2O_3–SiO_2 composite; J. Hazard. Mater. 185 (2011) 359-365.

[10] X. Zhong, S. Royer, H. Zhang, Q. Huang, L. Xiang, S. Valange, J. Barrault; Mesoporous silica iron-doped as stable and efficient heterogeneous catalyst for the degradation of C.I. Acid Orange 7 using sono–photo-Fenton process; Sep. Purif. Technol. 80 (2011) 163-171.

[11] T. Liu, H. You, Q. Chen; Heterogeneous photo-Fenton degradation of polyacrylamide in aqueous solution over Fe(III)–SiO_2 catalyst; J. Hazard. Mater. 162 (2009) 860-865.

[12] R. Molina, F. Martínez, J.A. Melero, D.H. Bremner, A.G. Chakinala; Mineralization of phenol by a heterogeneous ultrasound/Fe-SBA-15/H_2O_2 process: Multivariate study by factorial design of experiments; Applied Catalysis B: Environmental 66 (2006) 198-207.

[13] M. Ahmad, E. Ahmed, Z.L. Hong, W. Ahmed, A. Elhissi, N.R. Khalid; Photocatalytic, sonocatalytic and sonophotocatalytic degradation of Rhodamine B using ZnO/CNTs composites photocatalysts; Ultrasonics Sonochemistry 21 (2014) 761-773.

[14] Z. Zuo, R. Liao, X. Zhao, X. Song, Z. Qiao, C. Guo, A. Zhuang, Y. Yuan; Anti-frosting performance of superhydrophobic surface with ZnO nanorods; Applied Thermal Engineering 110 (2017) 39-48.

[15] P.M. Perillo, M.N. Atia, D.F. Rodríguez; Effect of the reaction conditions on the formation of the ZnO nanostructures; Physica E: Low-dimensional Systems and Nanostructures 85 (2017) 185-192.

[16] X. Yu, J. Zhang, X. Wang, Q. Ma, X. Gao, H. Xia, X. Lai, S. Fan, T.-S. Zhao; Fischer-Tropsch synthesis over methyl modified Fe_2O_3@SiO_2 catalysts with low CO_2 selectivity; Applied Catalysis B: Environmental 232 (2018) 420-428.

[17] W. Wei, Y. Ding, A. Zhao, K. Ge, C. Zhang, Y. Li, J. Zhang, G. Jia; Monodisperse and mesoporous walnut kernel-like SiO_2/γ-Fe_2O_3 nanocomposite: Synthesis, magnetic properties, and application in drug delivery; J. Alloys Compd. 728 (2017) 585-591.

[18] Y. Zhu, A. Apostoluk, P. Gautier, A. Valette, L. Omar, T. Cornier, J.M. Bluet, K. Masenelli-Varlot, S. Daniele, B. Masenelli; Intense visible emission from ZnO/PAAX (X = H or Na) nanocomposite synthesized via a simple and scalable sol-gel method; Scientific Reports 6 (2016) 23557.

[19] A.-T. Vu, V.-T. Vu; Preparation of MgO for Removal of Dyes and Heavy Metal from Aqueous Solution: Facially Controlling the Morphology, Kinetic, Isotherms and Thermal Dynamic Investigations; Indian Journal of Science and Technology, 11 (2018) 1-14.

.